Medical Engineering and Physics 120 (2023) 104045

Contents lists available at ScienceDirect

Medical Engineering and Physics

journal homepage: www.elsevier.com/locate/medengphy

Morphological characterisation of pediatric Turner syndrome aortae: Insights from a small cohort study

Lauren Johnston [a], Ruth Allen [b], Avril Mason [c], Asimina Kazakidi [a,*]

[a] Department of Biomedical Engineering, University of Strathclyde, Glasgow, UK
[b] Department of Radiology, Royal Hospital for Children, Glasgow, UK
[c] Department of Paediatric Endocrinology, Royal Hospital for Children, Queen Elizabeth University Hospital, Glasgow, UK

ARTICLE INFO

Keywords:
Turner syndrome
Aorta
Pediatric
Morphology
Hemodynamics
Cardiovascular

ABSTRACT

Cardiovascular disease is widespread in girls and women living with Turner syndrome (TS). Despite this prevalence, cardiovascular risk evaluation using the current guidelines has seen life-threatening aortic events occurring at dimensions classified within the normal threshold. In this study, we characterized the three-dimensional aortic geometries of Turner syndrome children and their age-matched healthy counterparts to evaluate various morphological parameters. Turner syndrome girls had overall greater values in ten out of fifteen parameters examined ($p > 0.05$), when compared to healthy children: the aortic arch height and width; the ascending aorta, aortic arch (2 locations), and descending aorta diameters; the ratio of the ascending to descending aorta diameter; average curvature; average torsion; and average curvature-torsion score. Additionally, significant associations were found in the TS group: body surface area and both arch height ($p = 0.03$) and arch height to width ratio ($p = 0.05$), and aortic arch diameter and both body surface area ($p = 0.04$) and weight ($p = 0.04$). The new information resulting from this small cohort study contributes to an improved understanding of the morphological parameters affecting the hemodynamic environment in TS, and the clinical assessment of the increased cardiovascular risk in this population.

1. Introduction

Turner syndrome is a multisystemic genetic disorder, with a deficiency of the second sex chromosome. Affected females (prevalence 1 in 2000 to 2500 worldwide [1,2]) have an increased predisposition for hypertension, atherosclerosis, and obesity, and Turner syndrome itself has been proposed as an independent risk marker for cardiovascular disease. In fact, approximately half of TS-affected women are born with a congenital cardiovascular defect [3–5]. Throughout the literature of Turner syndrome children (aged 2–19 years), the most common congenital heart defects were bicuspid aortic valve (29%), a dilated ascending aorta (19–22%), and aortic coarctation (11%) [6,7]. Congenital abnormalities of the aorta are discussed in more detail in a previous publication of ours [8]. Turner syndrome is associated with substantial morbidity, and a 3-fold (standardized mortality ratio, SMR = 3.0) higher mortality rate than the general population [9,10], with cardiovascular disease accounting for approximately half of all deaths [11].

Given the increased prevalence of cardiovascular disease in TS, clinical guidelines recommend a thorough cardiovascular examination of the heart and aorta at diagnosis [12]. Non-invasive cardiac imaging modalities, namely, transthoracic echocardiography (TTE), cardiovascular magnetic resonance imaging (CMR), and computed tomography (CT), are used to identify, diagnose, and monitor structural abnormalities of the heart. If initial imaging is normal, then NHS guidelines suggest this should be repeated every 5 years in children and every 10 years in adults [12]. If there is evidence of abnormalities such as bicuspid aortic valve, coarctation of the aorta, or dilatation of the ascending thoracic aorta, then annual imaging or follow-up imaging is advised [13].

Despite European [14] and American [12] guidelines, the cardiovascular risk stratification in Turner syndrome is challenging [15]. For example, aortic dissection (AoD), a severe cardiovascular complication that occurs more frequently and at a younger age in Turner syndrome patients, has been described in TS girls as young as 4 years of age [16]. Currently, the aortic size index (ASI = aortic diameter (cm)/body surface area (m^2)) is the primary method for estimating aortic dissection probability in TS patients and is routinely employed for clinical and

* Corresponding author.
E-mail address: asimina.kazakidi@strath.ac.uk (A. Kazakidi).

https://doi.org/10.1016/j.medengphy.2023.104045

Available online 29 August 2023

operative decision making. In adult women (> 18 years of age) with TS, the proposed threshold for aortic dissection risk is an ascending ASI greater than 2.5 cm/m^2 [17,18]. However, the characteristic short stature seen in TS complicates the assessment of AoD risk as the relationship of body size to aortic dimensions is different in Turner syndrome compared to the general population. ASI is also age-dependent and has been proven unreliable in younger children, with or without TS, due to the non-constant variance associated with rapid somatic growth [19]. In fact, ASI in the ascending aorta is often > 2.5 cm/m^2 in healthy girls with TS. Other studies predict AoD risk using the ratio of ascending to descending aortic diameter, with a value of > 1.5 indicating aortic dilatation [20]. However, this method does not consider that the descending aorta may be abnormal in TS females.

Cardiovascular risk assessment and prediction using the current guidelines has seen life-threatening aortic events occurring at dimensions classified as normal according to conventional size criteria [21]. This is due to a limited understanding of the pathophysiology of cardiovascular disease in TS and unreliable markers to predict cardiovascular risk. In 2018, the American Heart Association released a statement prioritizing research into the characterization of aortic enlargement, aneurysm, and dissection in TS. Prior to this statement, other authors had identified the importance of fully characterizing the cardiovascular anatomy in TS patients [6]. Therefore, in this study we aim to characterize the three-dimensional aortae of Turner syndrome, and healthy age-matched children, to improve our understanding of cardiovascular disease in this population.

2. Materials and methods

2.1. Patient cohorts

Ethical approval was obtained for a retrospective review of patients attending the pediatric Turner syndrome clinic at the Royal Hospital for Children, Queen Elizabeth University Hospital, Glasgow, UK. To be considered for this study, the patient had to have karyotypically proven Turner syndrome and retrospective cardiac imaging data obtained before the age of 18 years. Eight patients (n = 8, 14.3 ± 2.1 years, mean ± standard deviation) were identified that met the criteria (Table 1). Patient-specific volumetric image and geometrical data from four (n = 4) gender- and age-matched (12.5 ± 5.8 years, mean ± standard deviation) females was purchased from the Vascular Model Repository (www.vascularmodel.com). These models had no aortic abnormalities, and although BMI and blood pressure information was not provided, it is expected that these were within the normal range of a healthy child.

Table 1
Healthy and Turner syndrome baseline characteristics. Data shown as mean ± standard deviation. Hypertension was defined as systolic blood pressure ≥ 95th % for patient age and height. BMI category defined as normal weight (0 – 85th percentile), overweight (86th – 95th percentile), and obese (> 95th percentile).

	Healthy (n = 4)	Turner syndrome (n = 8)
Age (years)	12.5 ± 5.8	14.3 ± 2.1
Height (cm)	146*	142.4 ± 5.1
Weight (kg)	40.1*	54.2 ± 20.7
BSA (m^2)	1.2*	1.4 ± 0.2
BMI	19*	26.5 ± 9.1
BMI category		
- Normal weight	4 (100%)	4 (50.0%) [TS3, TS5, TS6, TS8]
- Overweight	0 (0.0%)	1 (12.5%) [TS1]
- Obese	0 (0.0%)	3 (37.5%) [TS2, TS4, TS7]
SBP (mmHg)	–	115 ± 15
DBP (mmHg)	–	66 ± 13
Hypertensive	0 (0.0%)	2 (25.0%) [TS4, TS8]
Aortic abnormality		
- Bicuspid aortic valve	0 (0.0%)	4 (50.0%) [TS1, TS6, TS7, TS8]
- Dilatation	0 (0.0%)	2 (25.0%) [TS1, TS8]
- Coarctation	0 (0.0%)	1 (12.5%) [TS3]
- Elongated arch	0 (0.0%)	2 (25.0%) [TS2, TS7]
- Gothic arch	0 (0.0%)	1 (12.5%) [TS5]
- Unconventional branching	0 (0.0%)	2 (25.0%) [TS4, TS7]

* *Information available for one healthy patient only from the Vascular Model Repository (www.vascularmodel.com).*

2.2. Image acquisition and geometry segmentation

Retrospective, anonymous, cardiac imaging data was obtained from each of the Turner syndrome girls outlined in Section 2.1. All cardiac imaging was performed between 2014–2018 on either a 1.5 Tesla diagnostic magnetic resonance imaging (MRI) scanner (MAGNATOM Aera/Avanto, Siemens Healthcare, GmbH), or a diagnostic revolution computed tomography (CT) scanner (GE Healthcare).

Image segmentation of the aorta was performed using the semi-automatic active contour-based algorithm implemented in ITK-SNAP. The aortic geometries were reconstructed such that only the ascending aorta (from above the location of the aortic root), aortic arch, descending aorta (to the end of the thoracic aorta), and the supra-aortic branches (brachiocephalic, left common carotid, and left and right subclavian branches) were kept. The output from the automated segmentation was visually inspected slice by slice and any artifacts were corrected with the manual segmentation tool within ITK-SNAP. This same methodology has been applied previously to segment aortic geometries from cardiac imaging data [22,23]. After segmentation, the surface models (stereolithography (STL) file-format) were smoothed in Autodesk Meshmixer (www.meshmixer.org) to remove surface artefacts prior to geometric analysis.

2.3. Morphometric analysis

Morphometric analysis was performed for all aortic geometries within the Vascular Modelling Toolkit (VMTK) (www.vmtk.org) software [24], an open-source collection of tools and libraries intended for geometric analysis of blood vessels. VMTK has previously been used to characterize geometrical changes in longitudinal studies of adults with Turner syndrome [25] and abdominal aortic aneurysms [26].

In VMTK, the centreline is automatically extracted in the form of a set of discrete points in space between the source and target point(s) – see Piccinelli et al. (2009) for further information [27]. In the case of the aorta, the centreline was computed from the ascending aorta (the source point) to the descending aorta (target point) (Fig. 1A). Before any analysis can be performed, the centreline coordinate data requires processing to remove any spurious values which may have been present as an artefact of voxel size or the segmentation process. Current approaches include the inbuilt VMTK centreline smoothing tool which applies a moving average filter and was implemented in Turner syndrome aortae by Subramaniam et al. [25], or the fitting of splines, specifically regression splines, which was implemented in this study, and that of Gallo et al. [23].

2.3.1. Morphological parameters

Morphometric analysis was performed for the full aortic geometry, and for anatomical subregions defined in the following paragraph (Fig. 1), in VMTK unless otherwise stated. First, the Euclidean distances, defined as the distance between the centreline and lumen wall, were computed. The Euclidean distance is useful in that it provides visual information on the dimensional (circumferential and axial) variation within and between patients. Previous studies have also employed this variable to visualize aortic growth in Turner syndrome women [25] and patients with small abdominal aortic aneurysms [26]. Single values were then computed for two- and three-dimensional parameters: vessel volume (V), surface area (SA), centreline length (l), arch height (H_{arch}), arch width (W_{arch}), and the subsequent ratio of height to width (H_{arch}/W_{arch}) (Fig. 1). Arch width was defined as the distance between the two centrelines in the ascending and descending aorta, at the cranial edge of the pulmonary artery, and height as the distance between the

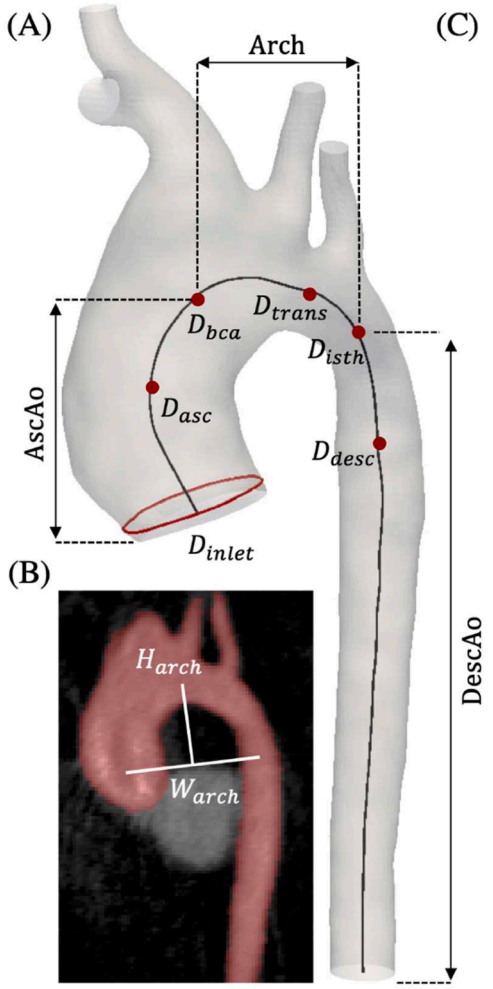

(C)

Morphological parameters

Volume: V

Surface area: A

Centerline length: l

Arch height, width, and height to width ratio: H_{arch}, W_{arch}, H_{arch}/W_{arch}

Shape index (ratio of min and max D): SI

Regional diameters: D_{asc}, D_{trans}, D_{isth}, D_{desc}

Diameter ratios: D_{asc}/D_{desc}, D_{trans}/D_{desc}, D_{isth}/D_{desc}

Curvature and torsion: k, τ

Combined curvature score: CC

Tortuosity: T

Fig. 1. Morphometric parameters exemplified (A, B) and listed (C) for the three-dimensional aorta of TS1. (A) Model centreline shown with regional points D_{asc}, D_{bca}, D_{trans}, D_{isth}, and D_{desc} as described in the text. (B) MRI slice showing the location of the arch width (W_{arch}) and height (H_{arch}) measurements, taken relative to the cranial edge of the pulmonary artery. (C) List of full morphological parameters.

imaginary line W_{arch} and the peak centreline point in the arch (Fig. 1B). Arch height and width are often computed in morphological studies of the aorta [28–30]. The height-to-width ratio is a parameter to characterize abnormal angulation and tortuosity of the arch. Finally, vessel curvature (k) and torsion (τ) were calculated, which at a given point on the centreline are the inverse of the radius of the osculating circle and the local deviation from the osculating plane, respectively. In other words, curvature measures the deviation of the centreline from an imaginary straight line, while torsion measures how sharp the centreline twists in 3D space [27,31].

$$k = \frac{|C'(s)\ x\ C''(s)|}{|C'(s)|^3} \quad \text{(Eq. 1)}$$

$$\tau = \frac{|C'(s)\ x\ C''(s) \cdot C'''(s)|}{|C'(s)\ x\ C''(s)|^2} \quad \text{(Eq. 2)}$$

where C is the centreline curve and s the curvilinear abscissa, while C' and C'' indicate the first and second derivatives of the curve with respect to the curvilinear abscissa. Both parameters are of interest considering their influence on the hemodynamics in the vasculature [32–35]. A third parameter which accounts for both curvature and torsion simultaneously is the combined curvature score (CC) proposed by O'Flynn [36]:

$$CC = \sqrt{k^2 + \tau^2} \quad \text{(Eq. 3)}$$

Computation of the vessel curvature, torsion, and combined curvature score is performed for every point along the centreline length; therefore, results were presented as minimum, maximum, and mean values. In addition, vessel tortuosity (T) defined as the ratio between centreline length (l) and the Euclidean distance between endpoints (d) was given as a single value for each geometry:

$$T = \frac{l}{d} - 1 \quad \text{(Eq. 4)}$$

For a more detailed, regional, analysis, the centreline length was divided at five locations relative to the individual model inlet diameter (D_{inlet}) and local landmarks (Fig. 1A). These were: in the ascending aorta, midway between the inlet and the aortic arch (D_{asc}); at the entrance to the aortic arch, proximal to the origin of the brachiocephalic branch (D_{bca}); in the transverse arch, midway between the left common carotid and left subclavian branches (D_{trans}); at the aortic isthmus, distal to the left subclavian branch (D_{isth}); and in the descending aorta, one inlet diameter downstream from the left subclavian branch (D_{desc}). The ascending aorta (AscAo) was defined as the region between the model inlet and D_{bca}, the arch as the region between R_{bca} and R_{isth}, and the descending aorta (DescAo) as the region from R_{isth} to the model end. The average and maximum values for diameter, curvature, torsion, and the combined curvature score were compared at each of these three regions.

2.3.2. Statistical analysis

Statistical analysis (Table 2) was performed on the morphometric parameters using OriginPro (version 2021b, OriginLab Corporation, USA) and Minitab Express (version 1.5.3, Minitab Inc, USA) software. To test for differences between the healthy and Turner syndrome groups, the univariate Mann–Whitney non-parametric U test was applied with the Significance level set at $\rho \leq 0.05$ [23]. For the Turner syndrome group only (due to a lack of data for the healthy girls), Pearson's correlation analysis was performed with the measured geometric parameters indexed to both body mass index (BMI) and body surface area (BSA).

3. Results

The complete set ($n = 12$) of in-scale three-dimensional aortic geometries is presented in Fig. 2A. As expected, and true for all geometries, the aortic diameter was greatest in the ascending aorta region and smallest at the aortic branches. The ascending aortic diameter was profoundly greater than the remainder of the aorta in TS1, TS6 and TS8. Note that TS1 and TS8 were diagnosed with aortic dilatation as per their clinical notes (Table 1). The maximum diameters seen within the healthy group ranged from 14.82 – 22.62 mm, whereas in the TS group these ranged from 17.72 – 32.56 mm (see supplementary material). When plotted along the centreline length it was clear the healthy group (Fig. 2B, H1–H4) displayed less variation in aortic diameter than the Turner syndrome group (Fig. 2C, TS1–TS8). Among the healthy group, the largest variation in aortic diameter was seen in H2 (D_{min}=15.00 mm and D_{max}=22.62 mm), compared to an average variation of 6.97 ± 0.93 mm (n = 4, mean ± standard deviation). Meanwhile in the TS group, the largest variation was seen in TS1 (D_{min} = 12.72 mm and D_{max} = 32.56 mm), compared to an average variation of 10.27 ± 4.67 mm (n=8, mean ± standard deviation).

Local curvature and torsion profiles highlight the non-uniformity and non-planarity of the aortic geometries. From Fig. 3A, peak curvature values (0.05 to 0.1 mm^{-1} depending on the individual) were clearly concentrated in the ascending aorta and arch regions, distal to the aortic valve. For all geometries, low curvature values (< 0.05 mm^{-1}) were found in the descending aorta (Fig. 3A). Inversely, there appeared to be less measured torsion ($\tau \sim 0$) in the proximal aorta (Fig. 3B). This was especially true for the healthy girls (H1–H4). Peak minimum (0 to −2 mm^{-1}) and maximum (0 to 2 mm^{-1}) torsion was predominantly visualized along the length of the descending aorta. The curvature and torsion data were then plotted along the centreline length for each individual (Fig. 4). For all individuals (healthy and Turner syndrome), peak curvature values occurred within 100 mm of the aortic valve, and torsion magnitude was greatest in the descending aorta. While there was no visible difference in curvature between the two groups, torsion values were marginally greater in the healthy group, but much more varied in the Turner syndrome group.

To directly compare the healthy and Turner syndrome data presented in Figs. 2–4, the diameter, curvature, torsion, and centreline length were non-dimensionalised. Aortic diameter was normalized with respect to the individual patient-specific inlet diameter, and centreline length, curvature, and torsion were normalized with respect to the maximum values. The average plus standard deviation was plotted for each group for the respective parameters: normalized diameter (Fig. 5A), curvature, (Fig. 5B), and torsion (Fig. 5C). Fig. 5A revealed a greater average normalized diameter among the healthy group, for all points along the centreline length. In other words, the average diameter throughout the aortic length was closer in value to the model inlet diameter for the healthy group. The difference between the two groups was most apparent in the ascending aorta and arch regions (normalized centreline length = 0.2 – 0.4) and least apparent in the descending aorta (normalized centreline length > 0.6). The variation around the group average (i.e., the standard deviation represented by the shaded region) was far greater among the Turner syndrome group, indicating larger variances in aortic diameter between each girl. The average normalized curvature presented in Fig. 5B shows a similar pattern for both patient groups: gradually increasing curvature directly distal to the aortic root (Fig. 5B, normalized centreline length: 0 – 0.1), followed by fluctuating higher curvature in the ascending aorta and arch (Fig. 5B, normalized centreline length: 0.1 – 0.4), and fluctuating lower curvature in the descending aorta (Fig. 5B, normalized centreline length = 0.4 –1). The normalized curvature was greater, on average, for the TS girls in the ascending and descending aorta, but not in the aortic arch. Fig. 5C presents the average pattern of normalized torsion, which was defined by small fluctuations around the zero value in the proximal aorta, and larger fluctuations in the distal descending aorta, for both patient groups. The average normalized torsion along the centreline length was predominantly greater for the healthy group, albeit both groups reached similar peak values for average torsion.

Statistical analysis was performed on three morphometric parameters known to influence hemodynamics, these being aortic diameter, curvature, and torsion (Fig. 6). Specifically, the average and maximum diameter (Fig. 6A, 6E), curvature (Fig. 6B, 6F), torsion (Fig. 6C, 6G), and the combined curvature torsion score (Fig. 6D, 6H), at three regions along the aorta, and along the full centreline length, were presented for both the healthy and TS groups (see supplementary material for the raw values). Median average (Fig. 6A) and maximum (Fig. 6E) diameter were greater in the TS group along the entire centreline length, and for each individual region. Almost all (5–95% as indicated by plot whiskers) of the healthy diameters were within approximately 5 mm s of the median value (Fig. 6A, E), unlike in the TS group where variability of diameter values was clearly greater (in Fig. 6A the ascending aorta and in Fig. 6E the ascending aorta, aortic arch, and the full model). Median average curvature (Fig. 6B) values were comparable between both groups at the ascending and descending aorta, and the full model. At the aortic arch region, median average curvature was marginally greater in the healthy group (Fig. 6B: 0.05 vs 0.045 1/mm). In the plot of

Table 2
Comparison of clinical and morphometric parameters averaged over the healthy ($n = 4$) and Turner syndrome groups ($n = 8$). Data presented as mean ± standard deviation. The Mann–Whitney U test was performed to determine if the values for each parameter were significantly different (significance values of $*p \leq 0.10$ and $**p \leq 0.05$) between the healthy and Turner syndrome groups. Note, there was not enough data available to perform this analysis for height or weight.

	Healthy ($n = 4$)	Turner syndrome ($n = 8$)	Mann–Whitney U test *P value*
Age (years)	12.5 ± 5.8	14.25 ± 2.12	0.31
Height (cm)	146.00	142.41 ± 5.08	–
Weight (kg)	40.10	54.21 ± 20.71	–
SBP (mmHg)	102 ± 2	115 ± 15	0.12
DBP (mmHg)	58 ± 3	66 ± 13	0.18
Volume (mm^3)	37,457 ± 17,023	59,725 ± 15,737	0.05 **
Surface area (mm^2)	11,207 ± 4,253	14,100 ± 2,134	0.28
l (mm)	185.40 ± 39.48	197.45 ± 20.59	0.57
H_{arch} (mm)	20.85 ± 5.10	21.31 ± 11.02	0.57
W_{arch} (mm)	38.88 ± 6.44	42.13 ± 9.70	0.37
H_{arch}/W_{arch}	0.54 ± 0.10	0.49 ± 0.20	0.39
D_{asc} (mm)	18.54 ± 3.21	23.18 ± 4.94	0.15
D_{trans} (mm)	16.18 ± 4.12	16.60 ± 1.77	0.79
D_{isth} (mm)	15.19 ± 4.03	15.56 ± 1.55	0.93
D_{desc} (mm)	14.24 ± 3.50	15.70 ± 1.62	0.68
$D_{asc/desc}$	1.32 ± 0.14	1.47 ± 0.24	0.21
$D_{trans/desc}$	1.14 ± 0.11	0.91 ± 0.38	0.15
$D_{isth/desc}$	1.06 ± 0.05	0.99 ± 0.10	0.15
SI (D_{min}/D_{max})	0.63 ± 0.03	0.58 ± 0.10	0.20
k_{mean} (mm^{-1})	0.02 ± 0.01	0.03 ± 0.00	0.07 *
τ_{mean} (mm^{-1})	−0.01 ± 0.01	0.02 ± 0.09	0.93
CC_{mean} (mm^{-1})	0.31 ± 0.19	0.47 ± 0.05	0.21
T	1.04 ± 0.37	0.79 ± 0.20	0.35

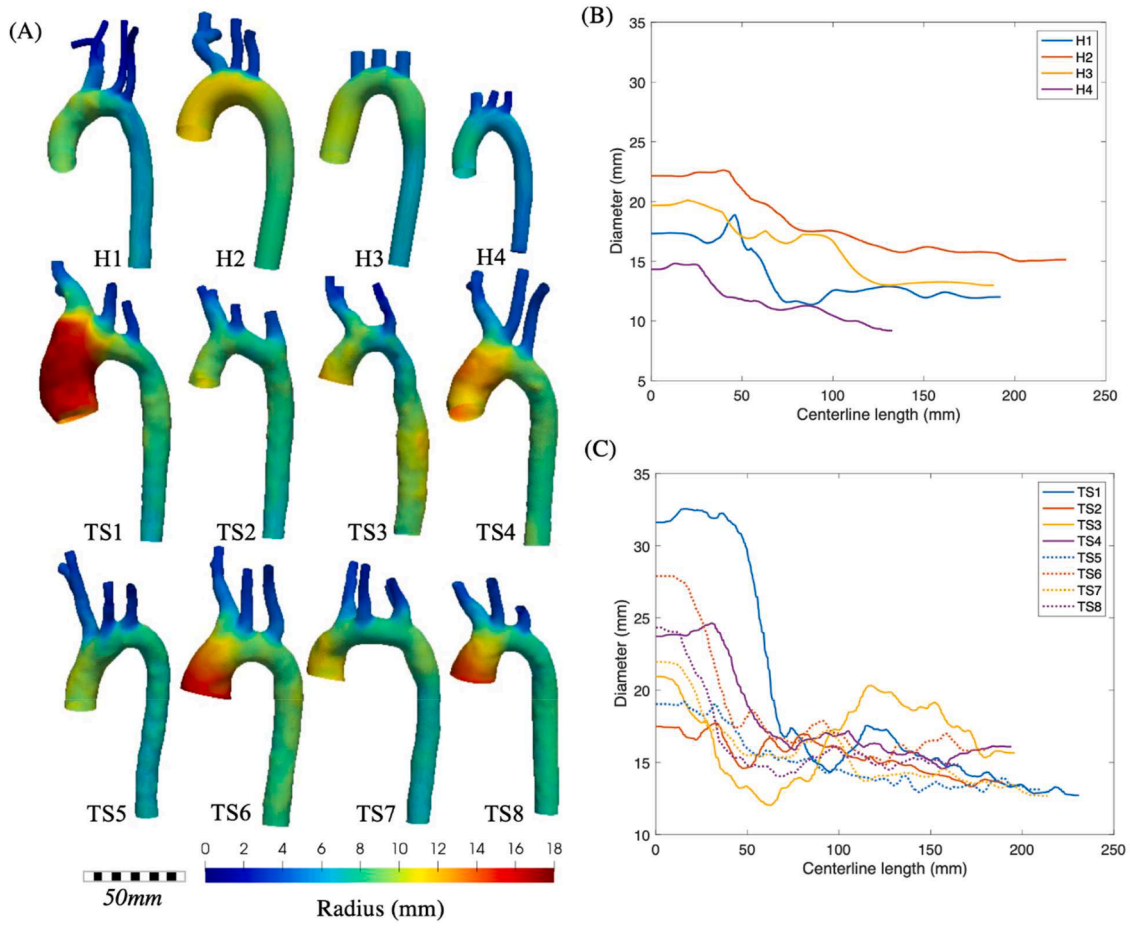

Fig. 2. (A) Colourmap distributions of the aortic radius and (B-C) line plots of the aortic diameter for the geometries of (H1–H4) healthy and (TS1–TS8) Turner syndrome (TS) girls. Geometries in (A) are shown in scale (anterior view). All values are in millimetres.

maximum curvature (Fig. 6F), the median values were distinctly greater for the healthy group at all regions investigated except for the ascending aorta where the difference was only marginal. For both groups, the average and maximum curvature was greatest in the aortic arch. Both average and maximum values for torsion (Fig. 6C, 6G) were greater for the healthy group at all regions considered with the exception of the average torsion in the ascending aorta (Fig. 6C). For both groups, the greatest torsion was seen in the descending aortic region (Fig. 6G). The distribution of combined curvature-torsion (CC) score followed a similar pattern for the average (Fig. 6D) and maximum results (Fig. 6H). That is, for the healthy group, the average and maximum CC values were greater at all regions considered. This difference was more pronounced in the descending region and for the full model, and less in the aortic arch and ascending aorta. The CC score results (Fig. 6D, H) were dominated by the respective torsion (Fig. 6C, G) values, which were substantially higher than the respective curvature values (Fig. 6B, F).

The parameters of interest (Fig. 1C) were averaged over the healthy ($n = 4$) and Turner syndrome groups ($n = 8$) and presented as the mean $\pm$ standard deviation in Table 2. The Mann-Whitney U test was then performed to determine if the values for both the healthy and Turner syndrome groups were statistically different ($p \leq 0.05$) (Table 2). Global parameters, these being the centreline length (l), arch height (H_{arch}), and arch width (W_{arch}), were greater in the Turner syndrome girls, but not significantly different (Table 2, $p = 0.37$–0.57) from the healthy group. The ratio of arch height to arch width (H_{arch}/W_{arch}) was greater in the healthy group, but not significantly different from the TS result (Table 2, $p = 0.39$). Further analysis was performed on the regional diameters (D_{asc}, D_{trans}, D_{isth} and D_{desc}) and the ratio of these diameters to the descending aorta ($D_{asc/desc}$, $D_{trans/desc}$, $D_{isth/desc}$) (Table 2). At all four regions, the Turner syndrome group had the greatest diameter, with the greatest difference between the two groups seen in the ascending aorta (Table 2, $D_{asc} = 23.18$ vs 18.54 mm). However, this difference was not statistically significant (Table 2, $p = 0.15$), nor was it for the other regional diameters (D_{trans}, D_{isth} and D_{desc}: $p = 0.68$–0.93). When the regional diameters were indexed to the descending diameter, $D_{asc/desc}$ was greater ($p = 0.21$) in the TS group but $D_{trans/desc}$ and $D_{isth/desc}$ were lower ($p = 0.15$). This was unsurprising as the TS group featured cases (Table 1) of ascending aortic dilatation, which would result in a higher $D_{asc/desc}$ ratio, and aortic coarctation, resulting in a lower $D_{trans/desc}$ and $D_{isth/desc}$ ratio. The same was true for the shape index (SI), the ratio of minimum to maximum diameter, where the larger diameters seen in the TS group resulted in a smaller SI value. Again, the statistical difference between the healthy and TS groups was not significant ($p = 0.20$). Finally, statistical analysis revealed that mean curvature (0.03 vs 0.02 mm^{-1}) and torsion magnitude τ_{mean} (0.02 vs -0.01 mm^{-1}) were greater in the Turner syndrome group, while tortuosity T was lower (0.79 vs 1.04 mm^{-1}). The mean curvature-torsion score CC_{mean} was also greater in the TS group (0.47 vs 0.31 mm^{-1}), which was expected as cumulative torsion was the dominant contributor. The healthy and TS values for k_{mean} were significantly different ($p = 0.07$) while for τ_{mean}, CC_{mean} and T there was no significant difference between the two groups (Table 2).

Further statistical analysis quantified the correlation between the investigated morphological parameters (Fig. 1) and clinical parameters such as body mass index, body surface area, weight, and systolic blood pressure (Table 3). This investigation was performed for the Turner syndrome group only due to a lack of data for the healthy group. When indexed to BMI, no statistically significant correlations were found. However, the result for D_{trans} (the diameter at the location of the

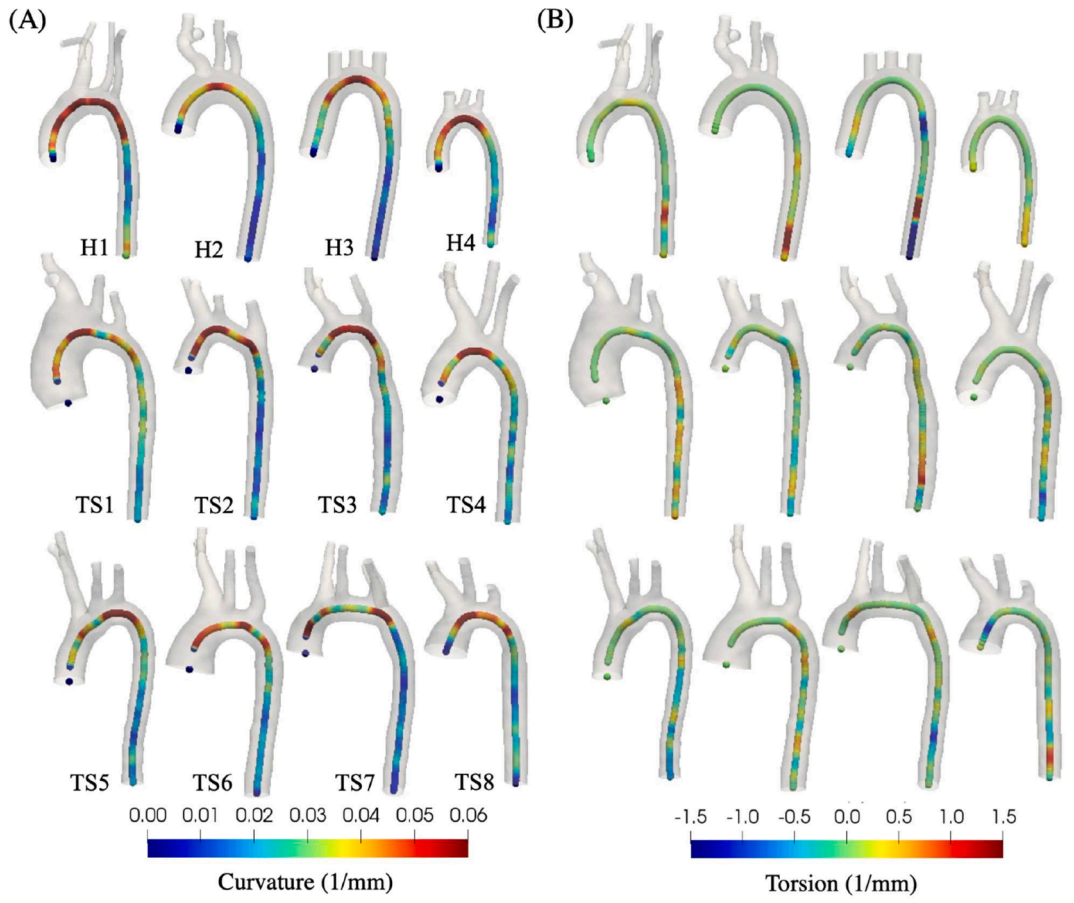

Fig. 3. Anterior view of the (A) curvature and (B) torsion for the geometries of the (H1–H4) healthy and (TS1-TS8) Turner syndrome girls. Geometries are in scale. All values are in millimetres^{-1}.

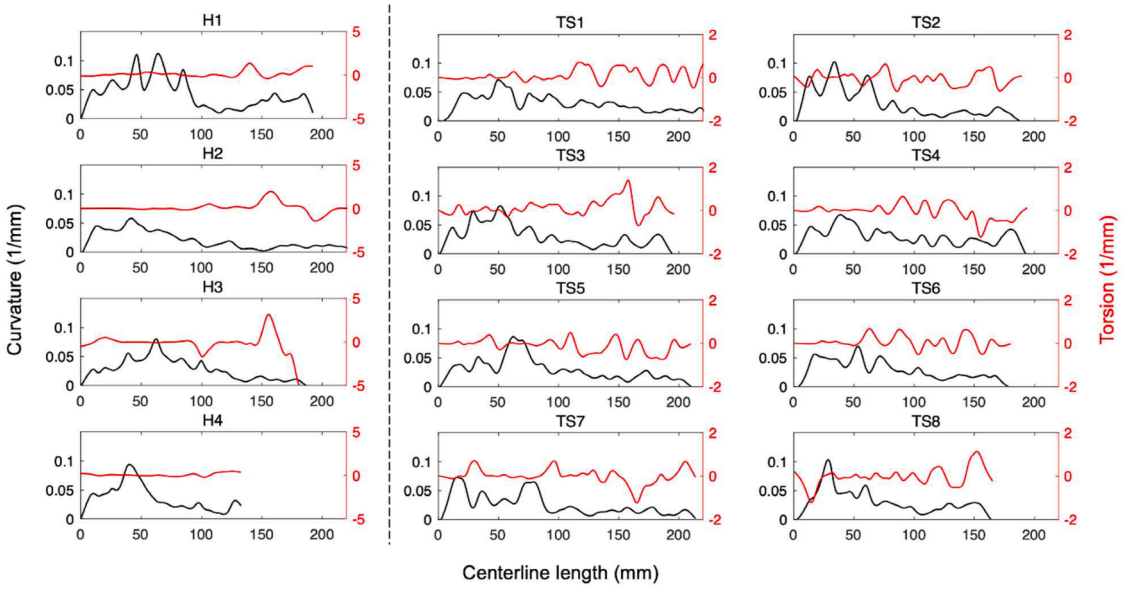

Fig. 4. Plots of the curvature (black line, primary y-axis) and torsion (red line, secondary y-axis) along the centreline length for each healthy (H1–H4) and Turner syndrome (TS1–TS8) girl. Note the difference in the torsion scale between the healthy (−5 to 5 mm^{-1}) and TS (−2 to 2 mm^{-1}) groups.

transverse arch, midway between the left common carotid and left subclavian) was very close with $p = 0.06$ (Table 3). When indexed to BSA, three parameters produced statistically significant correlations. These were H_{arch}, H_{arch}/W_{arch} and D_{trans} with p values of 0.03, 0.05 and 0.04 respectively (Table 3). Similarly, a significant correlation was found between D_{trans} and weight ($p = 0.04$). No significant correlations were found between systolic blood pressure and the investigated parameters (Table 3).

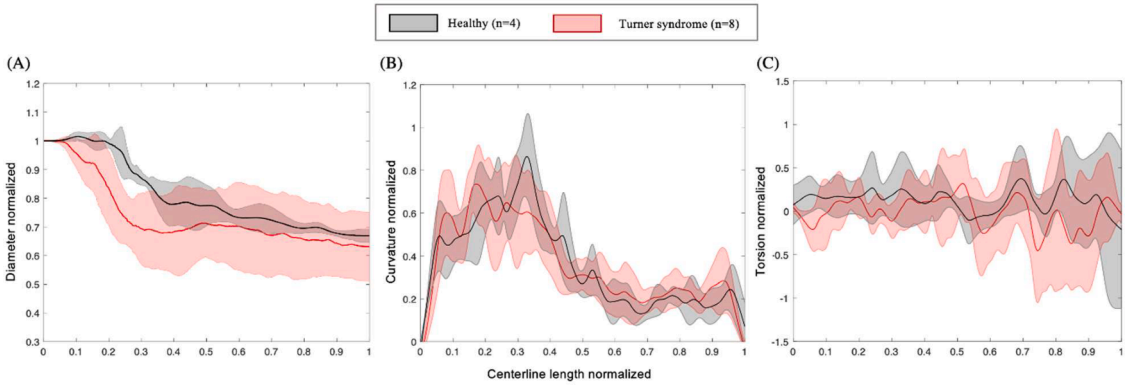

Fig. 5. Non-dimensional, normalized, data for (A) diameter, (B) curvature, and (C) torsion, plotted against the non-dimensional normalized centreline length for the healthy and Turner syndrome groups. Group average and standard deviation represented by the solid line and shaded region respectively. Diameter normalized with respect to the model inlet diameter, and centreline length, curvature, and torsion normalized with respect to the maximum values for each parameter.

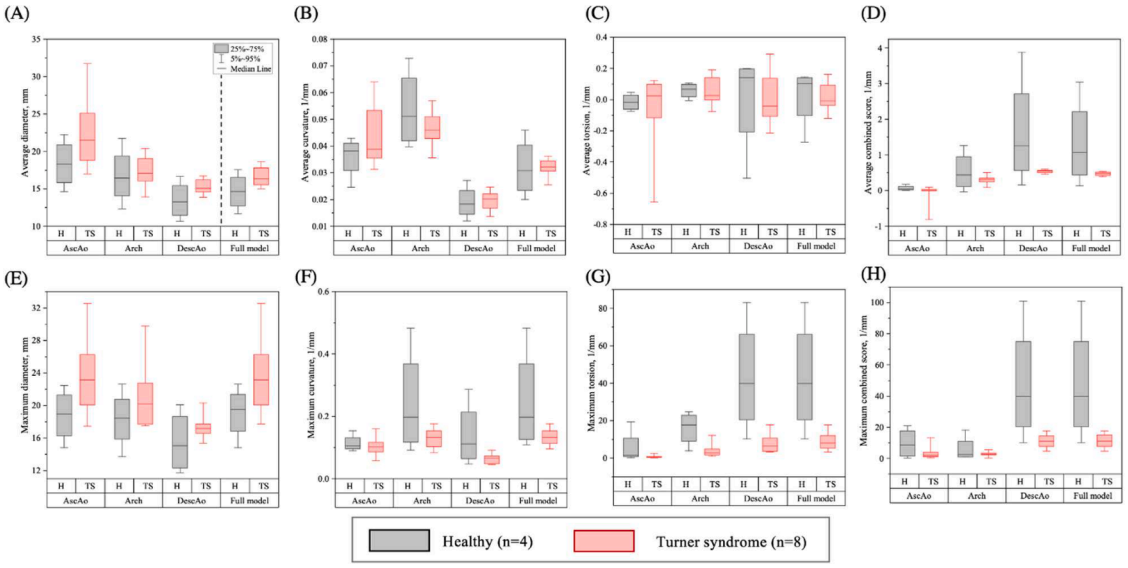

Fig. 6. Boxplots of average and maximum values for diameter (A, E), curvature (B, F), torsion (C, G), and the combined curvature torsion score (D, H) at four locations: ascending aorta, aortic arch, descending aorta, and the entire model. Results presented as the mean of the healthy (H1–H4) and Turner syndrome (TS1-TS8) groups, with the median value (horizontal line), interquartile range (box), and values for 95% coverage of the data (whiskers).

4. Discussion

In girls and women with Turner syndrome, congenital cardiovascular defects and acquired cardiovascular disease is common. As a result, the morphology of the ascending aorta, aortic arch, and descending aorta can be highly variable from patient to patient, in addition to varying incidences of dilatation, coarctation, non-uniformity, and non-planarity. Hemodynamic factors have been linked to the initiation and development of cardiovascular disease for decades, and the relationship between anatomical and hemodynamic factors is well known [37–41]. In this study, 3D models of the aortic arch were reconstructed from patient cardiac data, and morphometric parameters, defined by anatomical landmarks, were analysed to quantitatively define the three-dimensional morphology in a patient group with categorically abnormal aortic morphologies. This study complements a previous study [22] on the same patients which utilized computational fluid dynamic methods commonly used to analyse blood flow behaviour [42–44].

4.1. Clinical significance

Dimensional differences were observed both within the TS group and between the TS and healthy girls. The Euclidean distance maps (Fig. 2A) provided information on the variation in vessel radius, and highlighted areas with the greatest asymmetry. At all locations, Turner syndrome diameter was greater than respective healthy diameters (Fig. 6A,E and Table 2), which reflected the findings of similar studies on Turner syndrome children and adults [25,45]. The enlarged aortic diameters seen in this group may be due to the intrinsic abnormality of the intimal layer in the vascular wall, which is also observed in other genetic disorders (such as Marfan and Loeys–Dietz syndrome) where it is proven to lead to progressive dilation of the ascending aorta [46,47]. Identifying and/or diagnosing aortic dilatation in TS females is an important clinical step as it has been significantly associated with hypertension, even when age and BMI are accounted for [48]. Additionally, a similar link between ascending aorta dilatation and hypertension has been reported in disease-free individuals [49]. Two of the eight TS girls included in this study were clinically diagnosed with aortic dilatation (Table 1: TS1 and TS8). Of these two girls, only one (TS8) was also classed as hypertensive (138/88 mmHg). While TS1 did not have high blood pressure (116/75 mmHg), the severity of ascending aorta dilatation (even in comparison with other TS girls) may require prophylactic medical therapies earlier than what has been recommended for other conditions [12].

Table 3
Univariate regression of Turner syndrome parameters and body mass index (BMI), body surface area (BSA), weight, and systolic blood pressure (SBP). Significance values of $*p \leq 0.10$ and $**p \leq 0.05$.

	Indexed with BMI *P-value*	Indexed with BSA *P-value*	Indexed with weight *P-value*	Indexed with SBP *P-value*
Volume (mm^3)	0.83	0.98	0.92	1.00
Surface area (mm^2)	0.28	0.39	0.32	0.97
l (mm)	0.92	0.72	0.90	0.43
H_{arch} (mm)	0.11	0.03 **	0.07 *	0.53
W_{arch} (mm)	0.20	0.15	0.16	0.27
H_{arch}/W_{arch}	0.13	0.05 **	0.11	0.66
D_{asc} (mm)	0.69	0.66	0.69	0.51
D_{trans} (mm)	0.06 *	0.04 **	0.04 **	0.31
D_{isth} (mm)	0.18	0.31	0.24	0.84
D_{desc} (mm)	0.52	0.75	0.64	0.88
$D_{asc/desc}$	0.89	0.69	0.81	0.32
$D_{trans/desc}$	0.47	0.59	0.51	0.34
$D_{isth/desc}$	0.57	0.53	0.54	0.75
SI (D_{min}/D_{max})	0.81	0.70	0.78	0.68
k_{mean} (mm^{-1})	0.56	0.50	0.52	0.76
τ_{mean} (mm^{-1})	0.95	0.88	0.98	0.57
CC_{mean} (mm^{-1})	0.67	0.77	0.68	0.60
T	0.50	0.31	0.43	0.69

Interestingly, while TS4 was not diagnosed with aortic dilatation, this girl had the third largest ascending aorta diameter (Fig. 2A, C), a BMI of 47.4 and a systolic blood pressure of 136 mmHg (hypertensive). Aortic dilatation is also known to have an influence on flow rate, arterial resistance, and the presence of helical flow, especially in the ascending aorta [50]. The link between dilatation and disturbed blood flow was shown in our previous computational fluid dynamic study [22] which included some of the patient geometries presented here. Specifically, we observed highly disturbed flow with low velocity values in the dilated ascending aorta of TS1 along with low time-averaged wall shear stress at the proximal ascending aortic wall [22]. Furthermore, the degree of aortic dilatation and aortic growth rate are known to be risk factors for aortic dissection in similar genetic disorders such as the Marfan syndrome. Although it is uncertain whether the TS patients in this study would be more at risk for aortic dissection, patients with a high BMI (TS1, TS2, TS4 and TS7) and/or hypertension (TS4 and TS8) should probably be screened even if they do not meet the aortic size index criteria indicating a risk of dissection. Based on these risk factors, five of the eight Turner syndrome patients presented in this study would be flagged for dissection risk. When accounting for the common presence of bicuspid aortic valve in cases of TS dissection, TS6 would also be included in this higher-risk category [12,17].

4.2. Comparison with previous studies

Aortic arch morphology has been investigated in previous TS studies [48,51,52], where a significant association between either aortic arch morphology and hypertension [48], or abnormal arch morphology and blood pressure [51,53], have been reported. In this study, we quantified arch morphology according to aortic arch height, width, and the corresponding ratio, which is common in anatomical studies of the aorta [28–30]. Aortic arch height, width, and the ratio between the two (H_{arch}/W_{arch}) have been identified by several authors to influence pulse pressure and pulse wave velocity (PWV) in the aortic arch. Redheuil et al. [29] reported the significant relationship between increased arch width (W_{arch}), which we also saw in the TS group (Table 2) and increased PWV. Ou et al. [54] reported a similar positive relationship between an increased H_{arch}/W_{arch} (reminder: a higher H_{arch}/W_{arch} ratio is defined by a gothic shaped arch and increased central aortic stiffness, as well as enhanced systolic wave reflection. Both increased central aortic stiffness and enhanced systolic wave reflection are well-known contributors to the development of hypertension [55,56].The average ratio of aortic arch height to width was greater for the healthy group (0.54 ± 0.1) than the TS group (0.49 ± 0.2), however the maximum value across all individuals was seen in TS5 ($H_{arch}/W_{arch} = 0.92$). This was due to the abnormal angulation associated with a gothic shaped arch in TS5.

In this study, curvature and torsion averaged over the entire aortic centreline were greater in the TS group (Table 2). Subramaniam et al. [25], reported similar trends in their study measuring aortic dimensions in Turner syndrome adults. When looking at each region individually, median curvature values in the ascending and descending regions were greater in the TS group, meanwhile median curvature values in the arch were higher in the healthy group (Fig. 6B). The normalized curvature data followed a similar trend (Fig. 5B). On the other hand, median torsion values in the ascending aorta were greater in the TS group, and in the aortic arch and descending aorta, higher in the healthy group (Fig. 6C). While there does not appear to be any specific studies on aortic curvature and/or torsion in Turner syndrome, conclusions can be drawn from studies on patients with a similar genetic disorder, Marfan syndrome. Like Turner syndrome, Marfan syndrome (MS) is genetic disorder in which abnormal connective tissue composition predisposes the individual to aortic complications. A study by Poullis et al. [57] on Marfan syndrome patients, reported that aortic curvature had major effects on the forces exerted on the aortic wall. In fact, they suggested that aortic curvature was relatively more important that aortic diameter, blood pressure, cardiac output, and patient size with regard to the force acting on the aortic wall [57]. Given the predisposition of atherosclerotic lesions along the inner wall of curved segments, and the importance that flow-induced wall shear stress plays in the localization of atherogenesis [58–64], aortic curvature could be an important parameter to consider in risk stratification of Turner syndrome girls and women.

4.3. Limitations

There are some limitations present in this study. Firstly, we recognize that the sample size of 12 patients (4 healthy and 8 TS) included in this study is relatively small and it is likely that we did not account for the full range of morphological variability seen in the TS population. However, despite our small sample size, each TS aorta had some form of aortic abnormality, and we are therefore confident that the group of 8 TS girls provided a good representation of the population. Also, we can still extract some statistically significant results even if the group was small. Secondly, due to a lack of healthy clinical details with regards to height, weight, BMI, BSA, and blood pressure, unfortunately comparisons between the two groups could not be made for these parameters using the Mann–Whitney U test.

5. Conclusions and future work

In conclusion, we performed morphometric analysis of the aorta and supra-aortic branches in both healthy and Turner syndrome girls. Turner Syndrome is a rare disease, with a deficiency of the second sex chromosome. Because of this rarity, the studies currently available in the literature are limited. Thus, any new study that confirms and extends our current knowledge, providing further additional information is important in the clinical assessment of this patient population which uniquely presents very distinct aortic geometries. Our aim in this work was to identify differences between the healthy and TS groups, and to understand the clinical implications of morphologically abnormal aortic geometries. Turner syndrome girls had overall greater values in ten out of fifteen parameters examined (although not statistically significant, $p > 0.05$), when compared to an age- and sex-matched healthy group, that is: the aortic arch height and width; the ascending aorta, aortic arch (2 locations), and descending aorta diameters; the ratio of the ascending to descending aorta diameter; average curvature; average torsion; and average curvature-torsion score. These parameters may explain the

abnormal hemodynamics seen in Turner syndrome patients, namely vortical flow, flow separation, and flow disturbances, when compared to anatomically normal aortae, as shown in our previous study [22]. In addition, in the TS group a significant association between clinical (body surface area and weight) and morphological parameters (arch diameter, arch height and arch height-width ratio) was found. This small study lays out a framework that could be used for future machine learning algorithms to distinguish the TS aortas at risk for aortic dissection in large TS populations. Clinically, an improved understanding of the morphological parameters contributing to changes in the hemodynamic environment enhances our understanding of the increased risk of cardiovascular disease in this population. In the future, this area of research will need further studies with a larger cohort of patients and a broader age range.

Ethics statement

Full Ethical approval was awarded by the UK Health Research Authority (IRAS Project ID: 252,866, REC Reference: 18/LO/2052).

Funding

This work was supported in part by the UK Research and Innovation (UKRI) Engineering and Physical Sciences Research Council (EPSRC) Award Ref. 2104390 through the University of Strathclyde Research Studentship Scheme (SRSS) Student Excellence Awards (SEA) Project No 1619, the UKRI Natural Environment Research Council (NERC) Award Ref. NE/T014113/1, and the European Union's Horizon 2020 research and innovation programme under the Marie Sklodowska-Curie grant agreement No 749185. Asimina Kazakidi has received research grants from the UKRI EPSRC Award Ref. EP/W004860/1 and EP/X033686/1 via the Transformative Healthcare Technologies scheme. Funding for the open access publication fee were provided by UKRI through the above EPSRC and NERC projects.

CRediT authorship contribution statement

Lauren Johnston: Methodology, Formal analysis, Visualization, Conceptualization, Investigation, Data curation, Project administration, Software, Writing – original draft, Writing – review & editing. **Ruth Allen:** Resources, Data curation. **Avril Mason:** Resources, Data curation. **Asimina Kazakidi:** Conceptualization, Investigation, Data curation, Project administration, Supervision, Funding acquisition, Resources, Formal analysis, Methodology, Software, Visualization, Writing – review & editing.

Declaration of Competing Interest

The authors declare that the research was conducted in the absence of any commercial or financial relationships that could be construed as a potential conflict of interest.

Acknowledgments

The authors greatly acknowledge the support from the University of Strathclyde, the Royal Hospital for Children (Glasgow, UK), and the Queen Elizabeth University Hospital (Glasgow, UK).

Supplementary materials

Supplementary material associated with this article can be found, in the online version, at doi:10.1016/j.medengphy.2023.104045.

References

[1] Nielsen J, Sillesen I. Incidence of chromosome aberrations among 11148 newborn children. Humangenetik 1975;30:1–12. https://doi.org/10.1007/BF00273626.
[2] Nielsen J, Wohlert M. Chromosome abnormalities found among 34,910 newborn children: results from a 13-year incidence study in Arhus, Denmark. Hum Genet 1991;87:81–3. https://doi.org/10.1007/BF01213097.
[3] Sybert VP. Cardiovascular malformations and complications in Turner syndrome. Pediatrics 1998;101:E11. https://doi.org/10.1542/peds.101.1.e11.
[4] Mazzanti L, Cacciari E. Congenital heart disease in patients with Turner's syndrome. Italian study group for Turner syndrome (ISGTS). J Pediatr 1998;133:688–92. https://doi.org/10.1016/s0022-3476(98)70119-2.
[5] Völkl TMK, Degenhardt K, Koch A, Simm D, Dörr HG, Singer H. Cardiovascular anomalies in children and young adults with Ullrich–Turner syndrome the Erlangen experience. Clin Cardiol 2005;28:88–92. https://doi.org/10.1002/clc.4960280209.
[6] McCarthy K, Bondy CA. Turner syndrome in childhood and adolescence. Expert Rev Endocrinol Metab 2008;3:771–5. https://doi.org/10.1586/17446651.3.6.771.
[7] Chalard F, Ferey S, Teinturier C, Kalifa G. Aortic dilatation in Turner syndrome: the role of MRI in early recognition. Pediatr Radiol 2005;35:323–6. https://doi.org/10.1007/s00247-004-1359-5.
[8] Johnston L, Boumpouli M, Kazakidi A. Hemodynamics in the aorta and pulmonary arteries of congenital heart disease patients: a mini review. J Cardiol Cardiovasc Sci 2021;5:1–5. https://doi.org/10.29245/2578-3025/2021/2.1213.
[9] Stochholm K, Juul S, Juel K, Naeraa RW, Prevalence Højbjerg Gravholt C. Incidence, diagnostic delay, and mortality in Turner syndrome. J Clin Endocrinol Metab 2006;91:3897–902. https://doi.org/10.1210/jc.2006-0558.
[10] Schoemaker MJ, Swerdlow AJ, Higgins CD, Wright AF, Jacobs PA. United Kingdom clinical cytogenetics group. Mortality in women with Turner syndrome in Great Britain: a national cohort study. J Clin Endocrinol Metab 2008;93:4735–42. https://doi.org/10.1210/jc.2008-1049.
[11] Gravholt CH, Juul S, Naeraa RW, Hansen J. Morbidity in Turner syndrome. J Clin Epidemiol 1998;51:147–58. https://doi.org/10.1016/s0895-4356(97)00237-0.
[12] Silberbach M, Roos-Hesselink JW, Andersen NH, Braverman AC, Brown N, Collins RT, De Backer J, Eagle KA, Hiratzka LF, Johnson WH, et al. Cardiovascular health in Turner syndrome: a scientific statement from the American Heart Association. Circ Genom Precis Med 2018;11:e000048. https://doi.org/10.1161/HCG.0000000000000048.
[13] Hiratzka LF, Bakris GL, Beckman JA, Bersin RM, Carr VF, Casey DE, Eagle KA, Hermann LK, Isselbacher EM, et al. Guidelines for the diagnosis and management of patients with thoracic aortic disease: executive summary. Circulation 2010;121:1544–79. https://doi.org/10.1161/CIR.0b013e3181d47d48.
[14] Gravholt CH, Andersen NH, Conway GS, Dekkers OM, Geffner ME, Klein KO, Lin AE, Mauras N, Quigley CA, Rubin K, et al. Clinical practice guidelines for the care of girls and women with Turner syndrome: proceedings from the 2016 Cincinnati International Turner syndrome meeting. Eur J Endocrinol 2017;177:G1–70. https://doi.org/10.1530/EJE-17-0430.
[15] Marin A, Weir-McCall JR, Webb DJ, van Beek EJR, Mirsadraee S. Imaging of cardiovascular risk in patients with Turner's syndrome. Clin Radiolo 2015;70:803–14. https://doi.org/10.1016/j.crad.2015.03.009.
[16] Lippe BM, Kogut MD. Aortic rupture in gonadal dysgenesis. J Pediat 1972;80:895. https://doi.org/10.1016/S0022-3476(72)80162-8.
[17] Carlson M, Airhart N, Lopez L, Silberbach M. Moderate aortic enlargement and bicuspid aortic valve are associated with aortic dissection in Turner syndrome: report of the international turner syndrome aortic dissection registry. Circulation 2012;126:2220–6. https://doi.org/10.1161/CIRCULATIONAHA.111.088633.
[18] Matura LA, Ho VB, Rosing DR, Bondy CA. Aortic dilatation and dissection in Turner syndrome. Circulation 2007;116:1663–70. https://doi.org/10.1161/CIRCULATIONAHA.106.685487.
[19] Corbitt H, Maslen C, Prakash S, Morris SA, Silberbach M. Allometric considerations when assessing aortic aneurysms in Turner syndrome: implications for activity recommendations and medical decision-making. Am J Med Genet 2018;176:277–82. https://doi.org/10.1002/ajmg.a.38584.
[20] Lanzarini L, Larizza D, Prete G, Calcaterra V, Meloni G, Sammarchi L, Klersy C. Aortic dimensions in Turner's syndrome: two-dimensional echocardiography versus magnetic resonance imaging. J Cardiovasc Med 2007;8:428–37. https://doi.org/10.2459/01.JCM.0000269716.33435.d3.
[21] Mortensen KH, Andersen NH, Gravholt CH. Cardiovascular phenotype in Turner syndrome–integrating cardiology, genetics, and endocrinology. Endocr Rev 2012;33:677–714. https://doi.org/10.1210/er.2011-1059.
[22] Johnston L, Allen R, Hall Barrientos P, Mason A, Kazakidi A. Hemodynamic abnormalities in the Aorta of Turner syndrome girls. Front Cardiovasc Med 2021;8:670841. https://doi.org/10.3389/fcvm.2021.670841.
[23] Gallo D, Vardoulis O, Monney P, Piccini D, Antiochos P, Schwitter J, Stergiopulos N, Morbiducci U. Cardiovascular morphometry with high-resolution 3D magnetic resonance: first application to left ventricle diastolic dysfunction. Med Eng Phys 2017;47:64–71. https://doi.org/10.1016/j.medengphy.2017.03.011.
[24] Antiga L, Piccinelli M, Botti L, Ene-Iordache B, Remuzzi A, Steinman DA. An image-based modeling framework for patient-specific computational hemodynamics. Med Biol Eng Comput 2008;46:1097. https://doi.org/10.1007/s11517-008-0420-1.
[25] Subramaniam DR, Stoddard WA, Mortensen KH, Ringgaard S, Trolle C, Gravholt CH, Gutmark EJ, Mylavarapu G, Backeljauw PF. Gutmark-Little I. Continuous measurement of aortic dimensions in Turner syndrome: a cardiovascular magnetic resonance study. J Cardiovasc Magn Reson 2017;19:20. https://doi.org/10.1186/s12968-017-0336-8.

[26] Arzani A, Suh G-Y, Dalman RL, Shadden SC. A longitudinal comparison of hemodynamics and intraluminal thrombus deposition in abdominal aortic aneurysms. Am J Physiol-Heart Circ Physiol 2014;307:H1786–95. https://doi.org/10.1152/ajpheart.00461.2014.
[27] Piccinelli M, Veneziani A, Steinman DA, Remuzzi A, Antiga L. A framework for geometric analysis of vascular structures: application to cerebral aneurysms. IEEE Trans Med Imaging 2009;28:1141–55. https://doi.org/10.1109/TMI.2009.2021652.
[28] Boufi M, Guivier-Curien C, Loundou AD, Deplano V, Boiron O, Chaumoitre K, Gariboldi V, Alimi YS. Morphological analysis of healthy aortic arch. Eur J Vasc Endovasc Surg 2017;53:663–70. https://doi.org/10.1016/j.ejvs.2017.02.023.
[29] Redheuil A, Yu W-C, Mousseaux E, Harouni AA, Kachenoura N, Wu CO, Bluemke D, Lima JAC. Age-related changes in aortic arch geometry. J Am Coll Cardiol 2011;58:1262–70. https://doi.org/10.1016/j.jacc.2011.06.012.
[30] Sugawara J, Hayashi K, Yokoi T, Tanaka H. Age-associated elongation of the ascending aorta in adults. JACC: Cardiovasc Imaging 2008;1:739–48. https://doi.org/10.1016/j.jcmg.2008.06.010.
[31] Choi G, Cheng CP, Wilson NM, Taylor CA. Methods for quantifying three-dimensional deformation of arteries due to pulsatile and nonpulsatile forces: implications for the design of stents and stent grafts. Ann Biomed Eng 2009;37:14–33. https://doi.org/10.1007/s10439-008-9590-0.
[32] Browse NL, Young AE, Thomas ML. The effect of bending on canine and human arterial walls and on blood flow. Circ Res 1979;45:41–7. https://doi.org/10.1161/01.RES.45.1.41.
[33] Prosi M, Perktold K, Ding Z, Friedman MH. Influence of curvature dynamics on pulsatile coronary artery flow in a realistic bifurcation model. J Biomechan 2004;37:1767–75. https://doi.org/10.1016/j.jbiomech.2004.01.021.
[34] Smedby Ö, Bergstrand L. Tortuosity and atherosclerosis in the femoral artery: what is cause and what is effect? Ann Biomed Eng 1996;24:474–80. https://doi.org/10.1007/BF02648109.
[35] Wood NB, Zhao SZ, Zambanini A, Jackson M, Gedroyc W, Thom SA, Hughes AD, Xu XY. Curvature and tortuosity of the superficial femoral artery: a possible risk factor for peripheral arterial disease. J Appl Physiol 2006;101:1412–8. https://doi.org/10.1152/japplphysiol.00051.2006.
[36] O'Flynn PM, O'Sullivan G, Pandit AS. Methods for three-dimensional geometric characterization of the arterial vasculature. Ann Biomed Eng 2007;35:1368–81. https://doi.org/10.1007/s10439-007-9307-9.
[37] Chen J, Gutmark E, Mylavarapu G, Backeljauw PF. Gutmark-Little I. Numerical investigation of mass transport through patient-specific deformed aortae. J Biomech 2014;47:544–52. https://doi.org/10.1016/j.jbiomech.2013.10.031.
[38] Numata S, Itatani K, Kanda K, Doi K, Yamazaki S, Morimoto K, Manabe K, Ikemoto K, Yaku H. Blood flow analysis of the aortic arch using computational fluid dynamics. Eur J Cardiothorac Surg 2016;49:1578–85. https://doi.org/10.1093/ejcts/ezv459.
[39] Liu X, Pu F, Fan Y, Deng X, Li D, Li S. A numerical study on the flow of blood and the transport of LDL in the human aorta: the physiological significance of the helical flow in the aortic arch. Ame J Physiol-Heart Circul Physiol 2009;297:H163–70. https://doi.org/10.1152/ajpheart.00266.2009.
[40] Sundström E, Jonnagiri R, Gutmark-Little I, Gutmark E, Critser P, Taylor MD, Tretter JT. Effects of normal variation in the rotational position of the aortic root on hemodynamics and tissue biomechanics of the thoracic aorta. Cardiovasc Eng Tech 2020;11:47–58. https://doi.org/10.1007/s13239-019-00441-2.
[41] Pirola S, Jarral OA, O'Regan DP, Asimakopoulos G, Anderson JR, Pepper JR, Athanasiou T, Xu XY. Computational study of aortic hemodynamics for patients with an abnormal aortic valve: the importance of secondary flow at the ascending aorta inlet. APL Bioeng 2018;2:026101. https://doi.org/10.1063/1.5011960.
[42] Boumpouli M, Sauvage EL, Capelli C, Schievano S, Kazakidi A. Characterization of flow dynamics in the pulmonary bifurcation of patients with repaired tetralogy of fallot: a computational approach. Front Cardiovasc Med 2021;8:703717. https://doi.org/10.3389/fcvm.2021.703717.
[43] Boumpouli M, Danton MHD, Gourlay T, Kazakidi A. Blood flow simulations in the pulmonary bifurcation in relation to adult patients with repaired tetralogy of Fallot. Med Eng Phys 2020;85:123–38. https://doi.org/10.1016/j.medengphy.2020.09.014.
[44] Hyde-Linaker G, Barrientos PH, Stoumpos S, Kingsmore DB, Kazakidi A. Patient-specific computational haemodynamics associated with the surgical creation of an arteriovenous fistula. Med Eng Phys 2022;105:103814. https://doi.org/10.1016/j.medengphy.2022.103814.
[45] Baguet J-P, Douchin S, Pierre H, Rossignol A-M, Bost M, Mallion J-M. Structural and functional abnormalities of large arteries in the Turner syndrome. Heart 2005;91:1442–6. https://doi.org/10.1136/hrt.2004.048371.
[46] Gomez D, Al Haj Zen A, Borges LF, Philippe M, Gutierrez PS, Jondeau G, Michel J-B, Vranckx R. Syndromic and non-syndromic aneurysms of the human ascending aorta share activation of the Smad2 pathway: smad2 activation in ascending aortic aneurysm. J Pathol 2009;218:131–42. https://doi.org/10.1002/path.2516.
[47] Lin AE, Lippe BM, Geffner ME, Gomes A, Lois JF, Barton CW, Rosenthal A, Friedman WF. Aortic dilation, dissection, and rupture in patients with Turner syndrome. J Pediatr 1986;109:820–6. https://doi.org/10.1016/s0022-3476(86)80700-4.
[48] De Groote K, Devos D, Van Herck K, Demulier L, Buysse W, De Schepper J, De Wolf D. Abnormal aortic arch morphology in Turner syndrome patients is a risk factor for hypertension. Heart Vessels 2015;30:618–25. https://doi.org/10.1007/s00380-014-0529-0.
[49] Chrysohoou C, Skoumas J, Oikonomou E, Tsiachris D, Metaxa V, Lagoudakou S, Felekos J, Masoura C, Athanassopoulou S, Kosyfa H, et al. Aortic artery distensibility shows inverse correlation with heart rate variability in elderly non-hypertensive, cardiovascular disease-free individuals: the Ikaria Study. Heart Vessels 2013;28:467–72. https://doi.org/10.1007/s00380-012-0267-0.
[50] Frydrychowicz A, Berger A, Munoz del Rio A, Russe MF, Bock J, Harloff A, Markl M. Interdependencies of aortic arch secondary flow patterns, geometry, and age analysed by 4-dimensional phase contrast magnetic resonance imaging at 3 Tesla. Eur Radiol 2012;22:1122–30. https://doi.org/10.1007/s00330-011-2353-6.
[51] Ho VB, Bakalov VK, Cooley M, Van PL, Hood MN, Burklow TR, Bondy CA. Major vascular anomalies in Turner syndrome: prevalence and magnetic resonance angiographic features. Circulation 2004;110:1694–700. https://doi.org/10.1161/01.CIR.0000142290.35842.B0.
[52] Kim HK, Gottliebson W, Hor K, Backeljauw P, Gutmark-Little I, Salisbury SR, Racadio JM, Helton-Skally K, Fleck R. Cardiovascular anomalies in Turner syndrome: spectrum, prevalence, and cardiac MRI findings in a pediatric and young adult population. AJR Am J Roentgenol 2011;196:454–60. https://doi.org/10.2214/AJR.10.4973.
[53] Los E, Quezada E, Chen Z, Lapidus J, Silberbach M. Pilot study of blood pressure in girls with Turner syndrome: an awareness gap, clinical associations, and new hypotheses. Hypertension 2016;68:133–6. https://doi.org/10.1161/HYPERTENSIONAHA.115.07065.
[54] Ou P, Celermajer DS, Raisky O, Jolivet O, Buyens F, Herment A, Sidi D, Bonnet D, Mousseaux E. Angular (Gothic) aortic arch leads to enhanced systolic wave reflection, central aortic stiffness, and increased left ventricular mass late after aortic coarctation repair: evaluation with magnetic resonance flow mapping. J Thorac Cardiovasc Surg 2008;135:62–8. https://doi.org/10.1016/j.jtcvs.2007.03.059.
[55] London GM. Large artery function and alterations in hypertension. J Hypertens Suppl 1995;13:S35–8. https://doi.org/10.1097/00004872-199508001-00006.
[56] Willum-Hansen T, Staessen JA, Torp-Pedersen C, Rasmussen S, Thijs L, Ibsen H, Jeppesen J. Prognostic value of aortic pulse wave velocity as index of arterial stiffness in the general population. Circulation 2006;113:664–70. https://doi.org/10.1161/CIRCULATIONAHA.105.579342.
[57] Poullis MP, Warwick R, Oo A, Poole RJ. Ascending aortic curvature as an independent risk factor for type A dissection, and ascending aortic aneurysm formation: a mathematical model. Eur J Cardio-Thoracic Surg 2008;33:995–1001. https://doi.org/10.1016/j.ejcts.2008.02.029.
[58] Malek AM, Alper SL, Izumo S. Hemodynamic shear stress and its role in atherosclerosis. JAMA 1999;282:2035–42. https://doi.org/10.1001/jama.282.21.2035.
[59] Karino T, Asakura T, Mabuchi S. Role of hemodynamic factors in atherogenesis. Vascular endothelium in health and disease. Boston, MA: Springer US; 1988. p. 51–7. https://doi.org/10.1007/978-1-4684-8935-4_7. Advances in Experimental Medicine and Biology.
[60] Kazakidi A, Sherwin SJ, Weinberg PD. Effect of Reynolds number and flow division on patterns of haemodynamic wall shear stress near branch points in the descending thoracic aorta. J R Soc Interface 2009;6:539–48. https://doi.org/10.1098/rsif.2008.0323.
[61] Van Doormaal MA, Kazakidi A, Wylezinska M, Hunt A, Tremoleda JL, Protti A, Bohraus Y, Gsell W, Weinberg PD, Ethier CR. Haemodynamics in the mouse aortic arch computed from MRI-derived velocities at the aortic root. J R Soc Interface 2012;9:2834–44. https://doi.org/10.1098/rsif.2012.0295.
[62] Kazakidi A, Plata AM, Sherwin SJ, Weinberg PD. Effect of reverse flow on the pattern of wall shear stress near arterial branches. J R Soc Interface 2011;8:1594–603. https://doi.org/10.1098/rsif.2011.0108.
[63] Black SM, Maclean C, Hall Barrientos P, Ritos K, McQueen A, Kazakidi A. Calibration of patient-specific boundary conditions for coupled CFD models of the aorta derived from 4D Flow-MRI. Front Bioeng Biotechnol 2023;11:1178483. https://doi.org/10.3389/fbioe.2023.1178483.
[64] Black SM, Maclean C, Hall Barrientos P, Ritos K. Kazakidi A Reconstruction and validation of arterial geometries for computational fluid dynamics using multiple temporal frames of 4D Flow-MRI magnitude images. Cardiovasc Eng Technol 2023. https://doi.org/10.1007/s13239-023-00679-x.